Solar Energy Materials & Solar Cells 163 (2017) 43–50

Contents lists available at ScienceDirect

Solar Energy Materials & Solar Cells

journal homepage: www.elsevier.com/locate/solmat

Towards the implementation of atomic layer deposited In_2O_3:H in silicon heterojunction solar cells

Yinghuan Kuang[a,*], Bart Macco[a], Bora Karasulu[a], Chaitanya K. Ande[a], Paula C.P. Bronsveld[b], Marcel A. Verheijen[a], Yizhi Wu[a], Wilhelmus M.M. Kessels[a,c], Ruud E.I. Schropp[a,b,c]

[a] Department of Applied Physics, Eindhoven University of Technology, P.O. Box 513, 5600 MB Eindhoven, The Netherlands
[b] Energy research Center of the Netherlands (ECN), Westerduinweg 3, P.O. Box 1, 1755 ZG Petten, The Netherlands
[c] Solliance, High Tech Campus 21, 5656 AE Eindhoven, The Netherlands

ARTICLE INFO

Keywords:
Transparent conductive oxides
Atomic layer deposition
In_2O_3:H
Indium tin oxide
Silicon heterojunction solar cells

ABSTRACT

Hydrogen doped indium oxide (In_2O_3:H) with excellent optoelectronic properties, deposited using atomic layer deposition (ALD), has been made applicable as a window electrode material for silicon heterojunction (SHJ) solar cells. It is particularly challenging to integrate ALD In_2O_3:H into SHJ solar cells due to a low reactivity of the metalorganic precursor cyclopentadienyl indium (InCp) with the H-terminated surface of a-Si:H. This challenge has been overcome by a simple and effective plasma-based surface pretreatment developed in this work. A remote inductively coupled O_2 or Ar plasma has been used to modify the surface of a-Si:H, thereby promoting the adsorption of InCp on the surface. The impact of the short plasma exposure on c-Si/a-Si:H interface passivation has also been studied. It has been found that the observed degradation of the interface is not due to ion bombardment, but rather due to ultraviolet emission from the plasma. Fortunately, these light-induced defects have been found to be metastable, and the interface passivation can thus easily be fully recovered by a short post-annealing. Using such a mild Ar plasma pretreatment, ALD In_2O_3:H has been successfully implemented in a SHJ solar cell. A short-circuit current density of 40.1 mA/cm^2, determined from external quantum efficiency, is demonstrated for a textured SHJ solar cell with an In_2O_3:H window electrode, compared to 38.5 mA/cm^2 for a reference cell that has the conventional Sn-doped indium oxide (In_2O_3:Sn, ITO) window electrode. The enhanced photocurrent stems from a reduced parasitic absorption of In_2O_3:H in the entire wavelength range of 400–1200 nm.

1. Introduction

Transparent conductive oxides (TCOs) with excellent optoelectronic properties are vital to suppress optical losses in amorphous/crystalline silicon heterojunction (SHJ) solar cells and thereby attain a high energy conversion efficiency. In a conventional configuration of SHJ solar cells, with metal contacts both at the front and the rear side, parasitic absorption of light in the TCO and a-Si:H layers can be considered a substantial efficiency limiting factor [1,2]. Sn-doped In_2O_3 (In_2O_3:Sn, ITO), with a carrier mobility of 20–40 cm^2/(Vs) [3], is the most commonly used TCO in SHJ solar cells. The relatively high carrier density of 3–7×10^{20} cm^{-3}, however, causes a significant parasitic free carrier absorption and reflection in the red and near-infrared part of the solar spectrum [4,5]. More precisely, parasitic absorption in the ITO/a-Si:H layer stack at the front of a textured SHJ solar cell has been reported to account for photocurrent losses of 2.1 mA/cm^2 below 600 nm and 0.5 mA/cm^2 above 1000 nm [2]. Hydrogen-doped indium oxide (In_2O_3:H) has recently attracted great attention as a promising replacement for ITO. This is motivated by its superior transparency and low resistivity, which stem from its very high mobility (> 100 cm^2/Vs) and relatively low carrier density (< 2×10^{20} cm^{-3}) [4,6–8]. These excellent optoelectronic properties have made In_2O_3:H extremely interesting as a window electrode material for a variety of solar cells based on e.g. crystalline silicon (c-Si) [4,9,10], thin-film silicon [5,11], $Cu(In,Ga)Se_2$ (CIGS) [12,13], perovskite [14], perovskite/CIGS [15], and perovskite/c-Si [16] hybrid configurations.

In 2007, results on In_2O_3:H with a high mobility and low carrier density were first reported for magnetron sputtered layers from an In_2O_3 target, with introduction of water vapor during the deposition process [6]. Sputtered In_2O_3:H has since then been used successfully in SHJ cells, leading to excellent efficiencies. However, one of the main concerns related to sputtering is the damage induced to the a-Si:H/c-Si interface passivation by ultraviolet (UV) radiation and energetic ion-bombardment [17]. Atomic layer deposition (ALD), in contrast, can be

* Corresponding author.
E-mail address: y.kuang@tue.nl (Y. Kuang).

http://dx.doi.org/10.1016/j.solmat.2017.01.011
Received 24 August 2016; Received in revised form 6 January 2017; Accepted 9 January 2017
Available online 17 January 2017

employed to prepare the films without the damage by high-energy ions. In addition, ALD offers precise control over the film thickness at the atomic scale and conformal coating of thin films on complex substrate structures [18,19]. In 2011, Libera et al. [20] explored atomic layer deposition of In_2O_3 films using cyclopentadienyl indium (InCp) and a combination of oxygen and water as the reactants. Following the work of Koida et al. [6] and Libera et al. [20], we recently reported a two-step approach to prepare high mobility In_2O_3:H. In this approach, amorphous In_2O_3:H films were first deposited at 100 °C by ALD using precursors of InCp and a combination of both H_2O and O_2. Subsequently the films were post-annealed at 150–200 °C in nitrogen atmosphere for solid-phase crystallization. An excellent mobility of 138 $cm^2/(Vs)$, a moderate carrier density of 1.8×10^{20} cm^{-3}, and a low electrical resistivity of 2.7×10^{-4} Ω cm were demonstrated after crystallization by annealing at 200 °C for 30 min [8,21].

Despite the promising properties of the ALD In_2O_3:H layer, the integration of this material in SHJ solar cells has proven to be challenging. More precisely, it has been found that the ALD growth is completely inhibited on a H-terminated a-Si:H surface. Therefore, in this work we focus on overcoming this challenge. To this end, this paper is organized as follows. Firstly, it will be shown by X-ray Photoelectron Spectroscopy (XPS) measurements that the cause for the absence of ALD growth is the fact that the InCp precursor does not chemisorb on the a-Si:H surface. This points to a lack of reactivity between InCp and the H-terminated surface, which has been corroborated by density functional theory (DFT) calculations. Secondly, it will be shown that an inductively coupled plasma (ICP) based pretreatment can be employed to effectively alter the chemical nature of the H-terminated surface and thereby enable precursor adsorption. Although such a plasma pretreatment enables the ALD growth, it also leads to a degradation of the a-Si:H/c-Si interface passivation quality. Fortunately, it was found that the passivation quality can be completely recovered by thermal annealing. Using the mild plasma pretreatment, ALD In_2O_3:H was successfully integrated into SHJ solar cells, leading to a superior optical performance in the entire wavelength range of 400–1200 nm of spectral sensitivity of the device.

2. Materials and methods

2.1. Density functional theory calculations

Electronic structure calculations were performed using the generalized gradient approximation (GGA) to the density functional theory (DFT) [22,23] jointly with the Perdew–Burke–Ernzerhof (PBE) exchange correlation functional [24,25]. We also utilized the Grimme's DFT-D3 method including Becke-Jonson damping [26] to account for the non-bonded van der Waals interactions on an empirical basis. Further details of the DFT calculations and simulation models can be found in the Supporting Information. In addition, we computed the binding energies of InCp on various silicon surfaces through physisorption (ΔE_p) or chemisorption (ΔE_c) using Eq. (1).

$$\Delta E_{p/c} = E_{PS} - E_P - E_S \quad (1)$$

where E_{PS} is the total energy of the physisorbed/chemisorbed substrate-precursor complex, E_P and E_S are the total energies of an isolated InCp precursor and a given substrate surface. Here, physisorption can be described as the weak physical (non-covalent) binding of the InCp precursor on a given silicon surface, whereas the chemisorption requires the chemical (covalent) binding of indium that is likely accompanied by the decomposition of InCp.

2.2. Atomic layer deposition of In_2O_3:H on a-Si:H

Double-side polished (DSP) float-zone (FZ) n-type crystalline silicon (100) wafers (thickness: 280 μm, resistivity ρ: 2.5–3 Ω cm) were used as substrates. The wafers were first dipped in 1 vol% hydrofluoric acid (HF) for 1 min to remove the native oxide. Subsequently, 10 nm thick intrinsic a-Si:H layers were deposited on the wafers at a substrate temperature of 50 °C, using an inductively coupled Ar-SiH_4 plasma in a Plasmalab System100 from Oxford Instruments. Just before transferring to the ALD reactor for the plasma pretreatment, the c-Si/a-Si:H wafers were again dipped in 1 vol% HF for 1 min, to bring the surface in an H-terminated state.

The plasma pretreatment of a-Si:H was carried out at a temperature of 100 °C in an Oxford Instruments OpAL™ ALD reactor and consisted of exposure of the substrate to a remote inductively coupled O_2 or Ar plasma. If not particularly stated otherwise, a plasma power of 50 W and a pressure of 87 mTorr were used for the O_2 plasma, while 100 W and 109 mTorr were used for the Ar plasma.

Immediately following the plasma pretreatment, In_2O_3:H films were deposited at 100 °C in the same reactor, using InCp as the indium precursor and a mixture of H_2O and O_2 as co-reactants. This process was the same as described in our previous work [8]. The growth of In_2O_3:H on a-Si:H was monitored by in-situ spectroscopic ellipsometry (SE), and characterized by X-ray photoelectron spectroscopy (XPS).

The as-deposited In_2O_3:H films were annealed at 175 °C for 1 h in nitrogen atmosphere in a Jipelec rapid thermal anneal (RTA) for characterization of the optoelectronic properties. Film thickness and optical constants were evaluated by SE. A combination of a Tauc-Lorentz oscillator for the absorption across the optical band gap and a Drude oscillator for the free carrier absorption in the infrared part of the spectrum was used in the SE analysis. The electrical properties, i.e. carrier density N_e, mobility μ, and resistivity ρ were determined via Hall measurements in the Van der Pauw configuration. For the Hall measurements, In_2O_3:H was deposited on planar substrates, with a configuration of c-Si/SiO_2 (450 nm)/a-Si:H (intrinsic, 10 nm)/In_2O_3:H (77 nm). 71 nm thick ITO film deposited on an identical substrate was used as a reference to In_2O_3:H for the Hall measurements.

2.3. Plasma impact on c-Si/a-Si:H interface passivation

The impact of plasma pretreatment on the c-Si/a-Si:H interface passivation was evaluated by monitoring the minority carrier lifetime. n-type DSP FZ c-Si (100) wafers were passivated on both sides with 10 nm intrinsic a-Si:H, using an inductively coupled Ar-SiH_4 plasma at a substrate temperature of 50 °C. The wafers were subsequently annealed at 300 °C for 2 min in nitrogen in a Jipelec RTA before lifetime measurement. Shortly before and after the plasma pretreatment in the ALD reactor, and also after a following post-annealing, the lifetimes were characterized by means of photoconductance decay (PCD) measurements using a generalized mode at 20 °C in a Sinton WCT-120TS instrument. The effective lifetime was measured at an injection level of 10^{15} cm^{-3}.

2.4. Solar cell fabrication and characterization

For the fabrication of SHJ solar cells, textured n-type FZ c-Si (100) wafers (thickness: 280 μm, ρ: 2.5–3 Ω cm) were used as the base. Intrinsic (i) a-Si:H layers were first deposited on both sides of the textured wafer by plasma-enhanced chemical vapor deposition (PECVD) using a radio frequency (RF) of 13.56 MHz. Subsequently, n-type (n) and p-type (p) a-Si:H layers were deposited on the rear and the front, respectively, in the same PECVD system. The front TCO is In_2O_3:H by ALD as described above. For reference, ITO was deposited on companion cells by magnetron sputtering of an In_2O_3:SnO_2 (90:10 wt%) target at room temperature. The front Ag grids were fabricated by thermal evaporation. The cells of 2×2 cm^2 were isolated by laser scribing. The complete cell has a configuration of Ag/ITO/n/i/c-Si/i/p/TCO/Ag grids (rear to front).

Current density-voltage (J-V) measurements for the SHJ solar cells were performed using a Wacom dual-beam (halogen and xenon) solar

simulator calibrated to the AM1.5G spectrum (1000 W/m^2). Prior to the J-V measurements the cells were annealed at 175 °C for 1 h in nitrogen. External quantum efficiency (EQE) was measured with bias light under short-circuit conditions.

A cross sectional TEM sample of the SHJ solar cell was prepared using the Focused Ion Beam (FIB) lift-out technique. A protective Pt layer was deposited in two steps before FIB milling to protect the top surface from FIB induced damage. Subsequent TEM imaging was performed using a probe corrected JEOL ARM 200, equipped with a 100 mm^2 silicon drift detector (SDD) for energy dispersive X-ray spectroscopy (EDX). 2-dimensional EDX analysis was performed by acquiring full EDX spectra in an array of 256×256 pixels, at a 6,000,000× magnification, averaging over 44 full frames.

3. Results and discussion

3.1. Growth of ALD In_2O_3:H on a-Si:H

The nucleation of thin films in ALD processes is very much dependent on the interaction between precursor(s) and substrate surface. The nucleation will be challenging in case of insufficient interaction. As shown in Fig. 1, for up to 200 ALD cycles no growth of In_2O_3:H is observed on both HF-dipped c-Si and a-Si:H. Even when going up to 770 cycles only negligible In_2O_3:H thickness is obtained on the HF-dipped a-Si:H p-layer of the SHJ cell, as indicated by the photograph in the inset of Fig. 1. Growth of thin In_2O_3:H (dark brown color) on one edge of the cell is probably due to an incomplete removal of the native oxide at this edge. Also for an identical SHJ cell without HF dip, for up to 730 cycles only similarly negligible In_2O_3:H was obtained on the a-Si:H p-layer (not shown here). In contrast, a steady growth of In_2O_3:H on a 450 nm thick thermally grown SiO_2 layer is observed after an initial nucleation delay of 60–70 cycles. These observations demonstrate that understanding of the interaction between the precursor and the substrate surface is crucial for obtaining growth of In_2O_3:H on a-Si:H.

In order to understand the underlying mechanisms for the surface-dependent growth of In_2O_3:H, we employed ab initio DFT calculations to elucidate the interaction between the precursor and the substrate surface with different surface terminations. To this end, we created five surface models (Fig. 2) to account for the diverse cases: bare Si(111), Si-H, Si-OH, SiO_2(0001) (cleaved surface of α-quartz) and SiO_2-H. We report the binding energies computed using these models and the minimum-energy structures of the resulting physisorbed and chemisorbed species in Fig. 2.

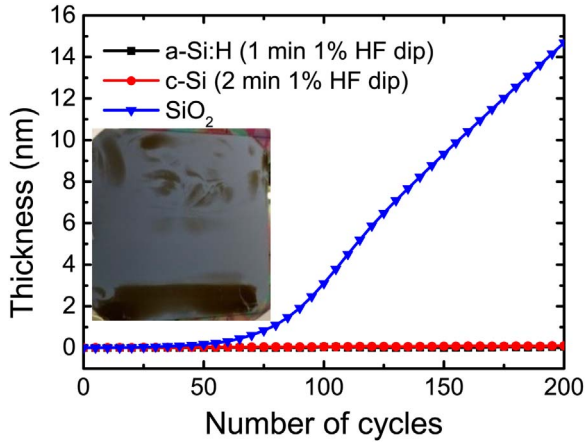

Fig. 1. Film thickness as a function of the number of ALD cycles during deposition of In_2O_3:H at a temperature of 100 °C on an HF-dipped c-Si wafer (labelled as c-Si) and c-Si wafers with either a 10 nm thick a-Si:H layer (labelled as a-Si:H) or a ~450 nm thick thermally grown SiO_2 layer (labelled as SiO_2). The inset photograph shows the front side of a 6″×6″ silicon heterojunction solar cell after 770 ALD cycles of In_2O_3:H. The c-Si, the a-Si:H, and the SHJ cell received an HF dip to remove native silicon oxide prior to the deposition of In_2O_3:H. Some areas of growth can be observed (dark brown color) in the photograph, but there is almost no growth on the most part of the a-Si:H p-layer (grey color). (For interpretation of the references to color in this figure legend, the reader is referred to the web version of this article.)

Judging from the DFT energies indicated in Fig. 2, we take note of the overall stronger binding of InCp on the bare surfaces (Si(111) and SiO_2) as compared to the H-/OH-terminated surfaces (Si-H, Si-OH and SiO_2-H). This can be ascribed to the ample dangling bonds residing on the bare surfaces. In particular, the bare SiO_2(0001) shows a notably strong InCp binding (−5.71 eV), consistent with the high reactivity of freshly-cut SiO_2, having a large surface energy of 2.2–2.4 J m^{-2} [27]. Accordingly, no stable physisorbed species could be obtained, as InCp is spontaneously chemisorbed on this highly reactive surface. For creating the bare SiO_2 surface (with unsaturated oxygens), a-Si:H surfaces can be treated with O_2 plasma that replaces the surface hydrogen with oxygen (Fig. 3). However, due to its high reactivity, bare SiO_2 was evinced (see Ref. [27] and references therein) to be readily hydrogenated/hydroxylated (forming SiO_2-H). We therefore anticipate that bare SiO_2 will primarily be hydrogenated in view of the availability of preexisting surface hydrogens (initially supplied by a-Si:H). Similar to SiO_2, a bare Si(111) surface exhibits an enhanced binding of InCp (−1.69 eV), albeit not as strong as SiO_2. However, being very reactive, also the bare Si(111) surface (e.g. c-Si) is unlikely to remain intact and will readily be hydrogenated or hydroxylated (creating Si-H or Si-OH groups).

As noted above, the Si-H, Si-OH and SiO_2-H surfaces are predicted to provide a weaker adsorption of InCp (Fig. 2), stemming from the passivating effect of the surface hydrogen. We expect that the abstraction of a proton from the surface by the Cp ligand would occur concertedly with the detachment of Cp, so as to facilitate the dissociative binding of InCp (Fig. 2). Even then, however, the chemisorption on either one of the considered H-/OH-terminated surfaces is not energetically as favorable as in the bare Si and SiO_2 surface cases. Among them, Si-H displays the weakest chemisorption of InCp (ΔE_c=−0.02 eV, Fig. 2) and the chemical conversion of the corresponding physisorbed species via proton transfer requires an energetically uphill process (ΔE=0.31 eV). This is expected to impede the covalent attachment of indium on the surface, and consequently the ALD nucleation, as endorsed by the negligible ALD growth rates on HF-dipped a-Si:H and c-Si samples even after numerous cycles (Fig. 1).

In contrast to Si-H, the hydroxylated surfaces (Si-OH and SiO_2-H) are expected to provide a stronger InCp chemisorption (Fig. 2). Si-OH groups might be formed in trace amounts (coexisting with Si-H groups) upon air exposure during the sample transfers, leading to a minor oxygen coverage (as demonstrated by XPS data, Fig. 4). The Si-OH surface is predicted to produce chemisorbed InCp products that are energetically less favorable than the physisorbed InCp species (ΔE=0.03 eV). This corresponds to a slightly endothermic process, which could hinder the ALD nucleation and growth. In accord with the DFT results, insignificant ALD growth is observed on the a-Si:H that is not pretreated with O_2 or Ar plasma (Fig. 3). Contrary to Si-OH, the dissociative binding of InCp on the SiO_2-H surface yields highly stabilized chemisorbed products (ΔE_c=−0.56 eV) through a feasible exothermic conversion process (ΔE=−0.30 eV). In line with these predictions, an early onset of growth of In_2O_3:H is observed on the (presumably H-terminated) SiO_2 surface that is either thermally-grown or created by O_2/Ar plasma pretreatments of a-Si:H (Figs. 1 and 3). Besides, the short nucleation delay of 60–80 ALD cycles before the proper film growth commences can be attributed to the time required for removing all hydrogen atoms passivating the surface oxygen atoms, through the likely mechanism wherein the hydrogen atoms are taken away by the Cp moieties. On account of the above experimental and simulated results, we conclude that surface modification of the a-Si:H is essential to enhance the reaction of InCp and thus stimulate the nucleation of In_2O_3:H on a-Si:H for SHJ solar cells.

To promote the adsorption of InCp molecules thereby stimulating

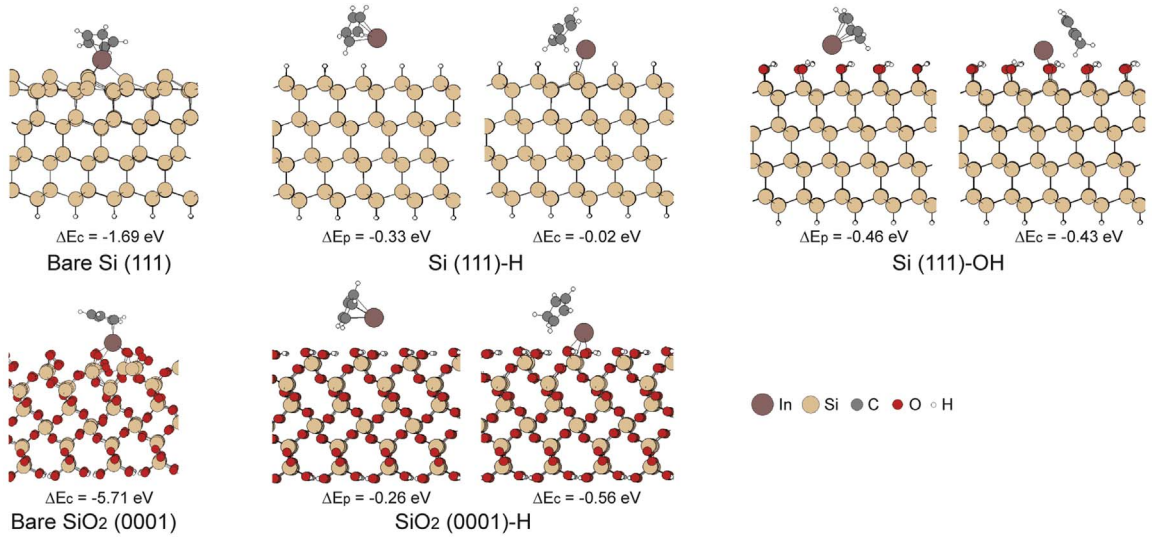

Fig. 2. DFT(PBE-D3)-level optimized structures of the physisorbed and chemisorbed InCp species on diverse silicon (oxide) surfaces. Computed relative energies for the physisorption (ΔE_p) and chemisorption (ΔE_c) of InCp on the surfaces are also indicated. For the bare Si(111) and the bare SiO_2(0001) surfaces, InCp spontaneously proceeds to the chemisorbed species due to the surface reactivity (only ΔE_c values).

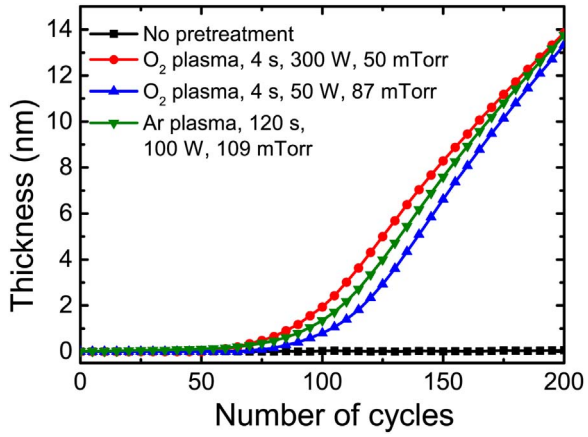

Fig. 3. Plasma pretreatment for nucleation of In_2O_3:H prepared by atomic layer deposition on a-Si:H. Inductively coupled O_2 or Ar plasma is used for surface pretreatment of the a-Si:H prior to the deposition of In_2O_3:H. The legend shows the plasma parameters, i.e. exposure time (s), RF power (W), and gas pressure (mTorr) for each type of plasma.

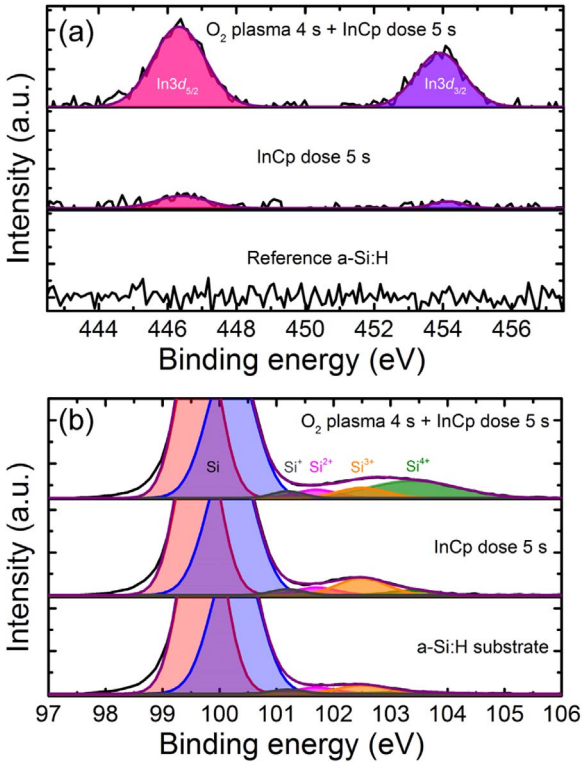

Fig. 4. XPS spectra of In 3*d* and Si 2*p* peaks for a-Si:H without treatment (reference), a-Si:H with only an InCp dosing of 5 s, and a-Si:H with an O_2 plasma pretreatment of 4 s, followed by an InCp dosing of 5 s (a) In 3*d* peaks, and (b) Si 2*p* peaks.

the nucleation of In_2O_3:H on a-Si:H, the a-Si:H was briefly exposed to either O_2 or Ar plasma. Fig. 3 demonstrates the effect of plasma pretreatment on the nucleation of In_2O_3:H on a-Si:H. Without the plasma pretreatment, no growth of In_2O_3:H on a-Si:H is observed. In contrast, with a short O_2 or Ar plasma exposure, growth of In_2O_3:H is obtained after a delay of 60–80 cycles. The steady growth of In_2O_3:H is only slightly further delayed by decreasing the plasma power from 300 W to 50 W when meanwhile increasing the gas pressure from 50 mTorr to 87 mTorr for the O_2 plasma.

The effect of plasma exposure on the adsorption of InCp on a-Si:H has also been investigated by XPS. As shown in Fig. 4a, it is clear that the adsorption of InCp on pristine a-Si:H is negligible, as indicated by the negligible intensity of the In 3*d* peaks. In contrast, with the O_2 plasma pretreatment of only 4 s prior to the InCp dosing, adsorption of InCp is markedly enhanced. This difference reveals that the plasma pretreatment is effective in stimulating the adsorption of InCp on a-Si:H.

To understand the surface modification of a-Si:H upon the O_2 plasma pretreatment, the various states of Si are probed by XPS, as shown in Fig. 4b. Si 2*p* peaks located at 99.8 eV for all the three samples are separated into Si $2p_{3/2}$ peak at ~99.6 eV and Si $2p_{1/2}$ peak at ~100.2 eV by Gaussian deconvolution. These strong peaks are assigned to the c-Si/a-Si:H substrate. The Si 2*p* peaks in the range of 101–105 eV are deconvoluted by Gaussian functions for multiple states of silicon [28–30]. After an O_2 plasma pretreatment of 4 s and a subsequent InCp dosing of 5 s the surface of a-Si:H is oxidized mainly to Si^{4+}, whereas with only InCp dose of 5 s lower states of Si^{2+} and Si^{3+} are the main products on the surface. The SiO_2 layer (Si^{4+}) created by the O_2 plasma on the a-Si:H remarkably enhances the adsorption of InCp molecules on the substrate (Fig. 4a). This observation is consistent with the DFT calculations (Fig. 2), which predicts the sufficient reactivity of InCp with SiO_2 surface for adsorption of the

precursor. A reference a-Si:H sample was loaded in the reactor for the same duration but without plasma treatment nor InCp dosing, to test the oxidation of the a-Si:H by background oxygen and water vapor in the reactor.

As for Ar plasma pretreatment, Si^{4+} is also the main state on the surface of a-Si:H after a plasma exposure of 120 s (XPS spectra not shown). The surface oxidation in this case could partly be ascribed to the background O_2 and H_2O in the reactor, since the reactor has only a moderately low base pressure of ~1 mTorr. In addition, the a-Si:H surface treated by the Ar plasma is likely to be quickly further oxidized in air during chamber opening and sample transport for the XPS measurement. Nevertheless, from the above results we conclude that the plasma exposure is an effective surface treatment to enhance the adsorption of InCp on a-Si:H, thereby initializing the nucleation of In_2O_3:H on surface-modified a-Si:H.

3.2. Impact of the plasma on the c-Si/a-Si:H interface passivation

In the previous section we have demonstrated that the plasma pretreatment is effective in modifying the surface of a-Si:H, thereby triggering the adsorption of InCp and initializing the nucleation of In_2O_3:H on a-Si:H. On the other hand, a detrimental influence of plasma exposure on c-Si/a-Si:H interface passivation should be avoided to obtain good electrical properties of SHJ solar cells. To this end, the passivation in terms of minority carrier lifetime was measured shortly before and after the plasma pretreatment. As shown in Fig. 5, both O_2 plasma (Fig. 5a) and Ar plasma (Fig. 5b–d) cause a degradation of the passivation. Lowering the gas pressure for the Ar plasma leads to a further passivation degradation (Fig. 5b and c). However, after a rapid annealing step at 300 °C in N_2 of only 1 min (Fig. 5a and b) or a low-temperature annealing treatment at 175 °C for 1–2 h (Fig. 5d), the degradation is annealed out. Only the degradation caused by the low pressure Ar plasma (Fig. 5c) cannot be completely repaired under the same annealing conditions. The temperature of 175 °C and the annealing duration of 1 h shown in Fig. 5d represent the post-annealing conditions used for the actual solar cells present in this work, as indicated in Experimental Section 2.4. The configuration of the semi-cells tested in Fig. 5 incorporates the critical a-Si:H/c-Si interfaces as also present in the actual solar cell devices. Therefore a similar damage recovery upon annealing can be expected in the solar cells.

The carrier lifetime degradation could be ascribed to the creation of metastable defects in a-Si:H [31]. The H-passivated dangling bonds can convert into metastable defects by both light illumination and ion bombardment, leading to a degradation of the passivation state [32–34]. The degradation is recovered once the hydrogen atoms obtain sufficient energy during the post-annealing to diffuse to the neighboring dangling bonds within the a-Si:H network and terminate the metastable defects [31]. From the results shown in Fig. 5, we can conclude that by using mild plasma conditions, i.e. a combination of high gas pressure and low RF power for the remote inductively coupled Ar plasma, no permanent damage on the c-Si/a-Si:H interface passivation remains after post-annealing.

To further investigate the mechanisms for the plasma-induced degradation of the minority carrier lifetime, the vacuum ultraviolet (VUV, 100–200 nm) and UV (200–400 nm) emission of the inductively coupled O_2 plasma and Ar plasma was studied by optical emission spectroscopy (OES). Details of the OES measurements are described elsewhere [35]. The emission spectra are shown in Fig. 6a and b. Both the plasmas have intense emission peaks in the VUV region. For a more detailed study, the O_2 plasma is chosen to distinguish the degradation of passivation by optical radiation from that by ion bombardment. Accordingly, an optical filter of either MgF_2 or quartz was placed directly on top of the c-Si/a-Si:H wafer. The filter excludes ion bombardment and any other potential direct reactions of the O_2 plasma with the a-Si:H surface. Because of the band gap, the quartz filter blocks the photons with wavelengths < 140 nm (> 8.9 eV), whereas the MgF_2 filter blocks the photons with wavelengths < 110 nm (> 11.3 eV) while it has ~60% transmittance at the emission peak of 130.5 nm (9.5 eV) of the O_2 plasma [35]. To assure a clear trend of lifetime degradation, we intentionally used a relatively high

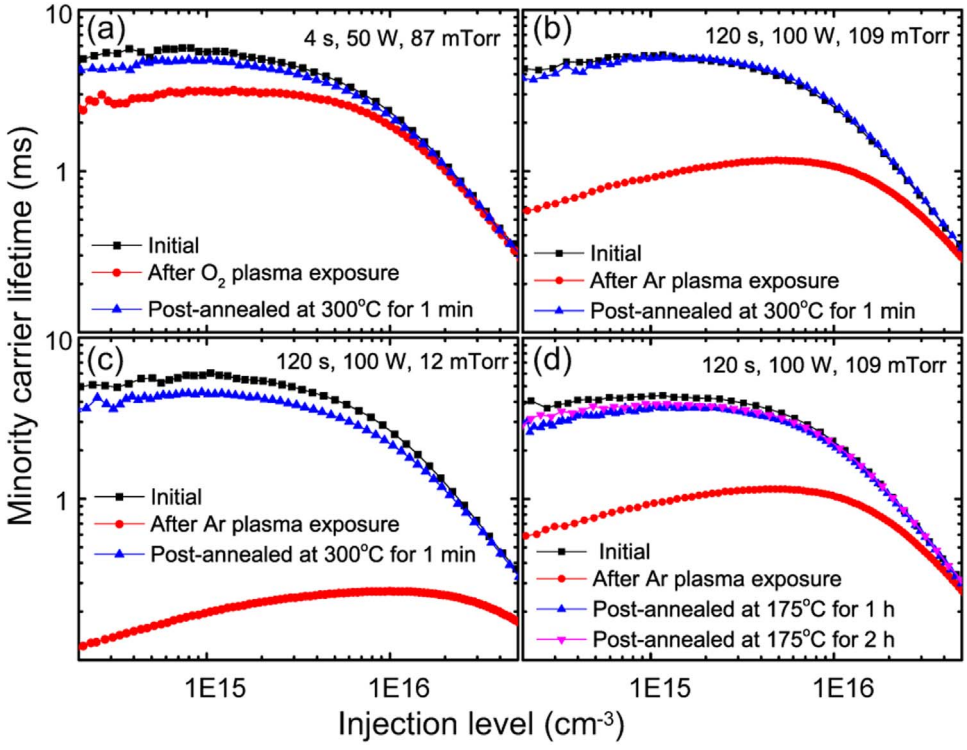

Fig. 5. Minority carrier lifetimes of c-Si wafers passivated by 10 nm thick a-Si:H layers at both sides. The lifetimes were measured before and after plasma pretreatment, and after a subsequent post-annealing step. Inductively coupled O_2 or Ar plasma was used for the pretreatment: (a) O_2 plasma. (b) Ar plasma, high pressure. (c) Ar plasma, low pressure. (d) Ar plasma, low post-annealing temperature of 175 °C. The plasma parameters including exposure time (s), RF power (W), and gas pressure (mTorr) are indicated in each graph.

power of 300 W and a low pressure of 30 mTorr. Fig. 6c shows the influence of O_2 plasma exposure on the minority carrier effective lifetime. With the ion flux blocked by the MgF_2 filter while allowing the VUV and UV photons to reach the substrate, the lifetime degradation (corrected for the ~60% photon transmittance at 130.5 nm) is approximately the same as that for the sample for which the ion flux was not blocked (no filter). This means that the degradation does not notably differ for the situations with and without filter. Therefore we can conclude that the ion bombardment plays a negligible role while the photons play a dominant role in the observed lifetime degradation. When the photons at 130.5 nm are blocked by the quartz filter, substantially less degradation of the lifetime is observed than that with the MgF_2 filter. This difference suggests that the VUV emission plays a predominant role in lifetime degradation during the plasma exposure. We note that a similar conclusion was drawn by Lebreton et al., via exposure of c-Si wafers passivated by a-Si:H to various capacitively coupled plasmas of Ar, Ar-H_2, and H_2 [31].

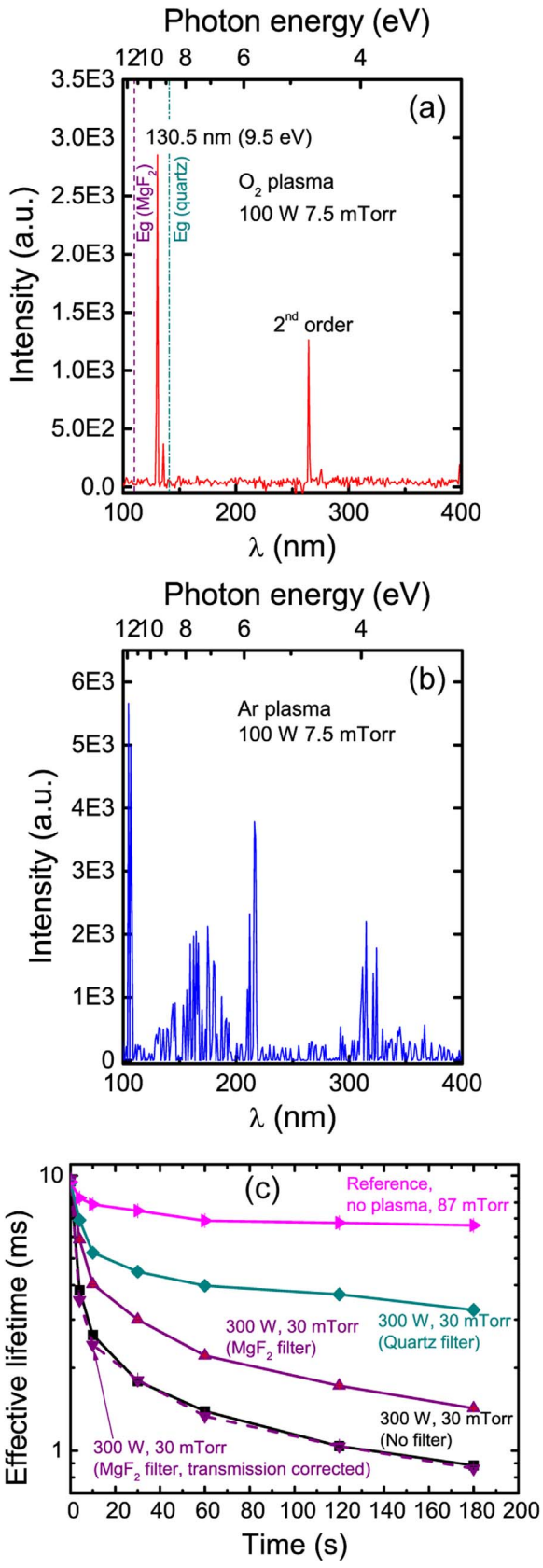

Fig. 6. Emission spectra of inductively coupled O_2 plasma (a) and Ar plasma (b), measured in the vacuum UV (100–200 nm) and UV (200–400 nm) region. The second order peak at 260 nm for O_2 plasma is caused by the diffraction grating in the monochromator and is associated with the 130.5 nm emission line [35]. (c) Minority carrier effective lifetime at an injection level of 10^{15} cm^{-3} as a function of O_2 plasma exposure time for c-Si wafers passivated by ~12 nm thick a-Si:H layers at both sides. Lifetimes are also given for the substrates capped by optical filters which block (Quartz) or transmit (MgF_2, with and without correction of the 60% transmission at 130.5 nm) the vacuum UV emission of O_2 plasma at 130.5 nm. A sample loaded in the reactor without plasma exposure is included as a reference.

3.3. SHJ solar cell with In_2O_3:H

Excellent electrical properties of ALD In_2O_3:H on a-Si:H have been demonstrated by Hall measurements. The as-deposited In_2O_3:H (77 nm in thickness) in this study exhibits a carrier density of 1.8×10^{20} cm^{-3}, a carrier mobility of 66 cm^2/V s, and a resistivity of 5.2×10^{-4} Ω cm. After annealing at 175 °C for 1 h in N_2 these parameters are improved to 1.4×10^{20} cm^{-3}, 104 cm^2/V s, and 4.4×10^{-4} Ω cm, respectively. For comparison, a carrier density of 6.3×10^{20} cm^{-3}, a carrier mobility of 26 cm^2/V s, and a resistivity of 3.7×10^{-4} Ω cm are determined for the ITO (71 nm in thickness) on a-Si:H, which was annealed simultaneously with the In_2O_3:H. The combination of low carrier density and high mobility is beneficial for minimizing the free carrier absorption without sacrificing the electrical conductivity of the In_2O_3:H.

To test its optoelectronic performance in devices, ALD In_2O_3:H has been implemented into SHJ solar cells. Ar plasma pretreatment (exposure duration: 120 s, RF power: 100 W, gas pressure: 109 mTorr) was used for the surface treatment of a-Si:H p-layer. Ar plasma is chosen rather than O_2 plasma because of the reduced oxidation of a-Si:H, thereby avoiding a tunneling barrier at the a-Si:H/In_2O_3:H interface. Fig. 7a shows the illuminated current density-voltage (J-V) characteristics of the SHJ solar cells with an ~80 nm thick In_2O_3:H or ITO window electrode. With respect to ITO, the In_2O_3:H demonstrates a photocurrent gain of 1.7 mA/cm^2 for the SHJ cell. This current gain stems mainly from the reduced parasitic absorption of the In_2O_3:H in the entire wavelength range of 400–1200 nm, as indicated by the EQE measurements shown in Fig. 7b and as confirmed by absorption spectra determined by both spectroscopic ellipsometry and UV–VIS–NIR spectroscopy (Fig. S1 in the Supporting Information). Consequently, a remarkably high photocurrent density of 40.1 mA/cm^2 was determined from EQE for the cell with In_2O_3:H electrode, compared to 38.5 mA/cm^2 for its counterpart with ITO. These values are consistent with those obtained from the light J-V measurements. The overall efficiency remains rather low however, which is related to the low fill factor and relatively low V_{oc} for both the reference cell and the cell with In_2O_3:H. Although further study on these aspects are required to obtain efficient SHJ solar cells, the present cells allow to validate the beneficial optoelectronic properties of ALD In_2O_3:H.

To study the microstructure of In_2O_3:H on a-Si:H in the SHJ cell, a cross section of the c-Si/a-Si:H/In_2O_3:H layer stack was imaged by

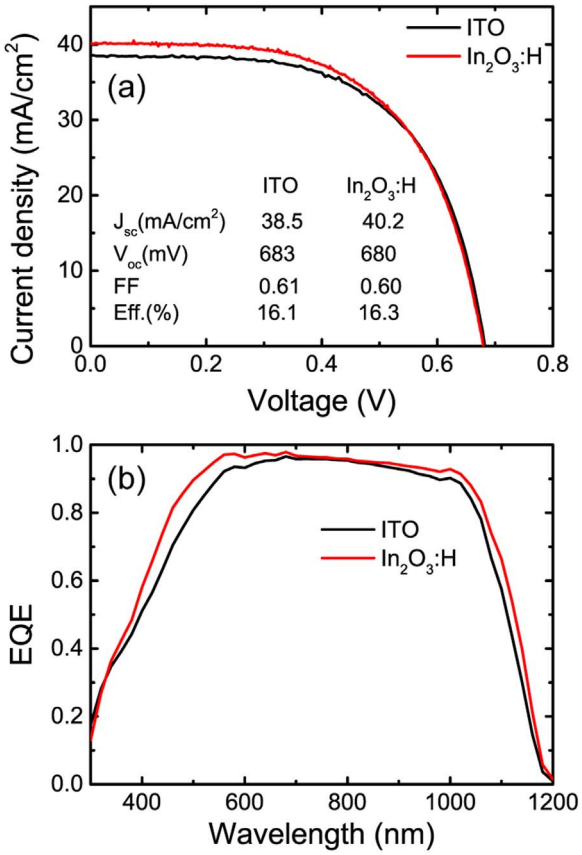

Fig. 7. (a) Light J-V characteristics of silicon heterojunction solar cells with sputtered ITO and atomic layer deposited In_2O_3:H window electrodes. (b) The corresponding external quantum efficiency curves.

TEM. A homogenous coverage of ALD In_2O_3:H on the textured substrate, even in the valley region of c-Si pyramids, can clearly be seen in Fig. 8a. In the zoomed-in high-resolution TEM image (Fig. 8b), a sharp c-Si/a-Si:H interface is distinguishable, which is beneficial for the passivation of interface states [36]. In_2O_3:H grains of ~50–100 nm in the lateral direction can be distinguished in Fig. 8c. A compositional profile across the layer stack indicates a rather diffuse a-Si:H/In_2O_3:H interface (Fig. 8d). This can either be ascribed to the presence of an In-Si-O alloy due to inter-diffusion at the interface, or to the projection of two phases, separated by the rough interface, on top of each other. Due to the interface roughness it is rather difficult to distinguish a SiO_2 phase present at the a-Si:H/In_2O_3:H interface.

4. Conclusions

In_2O_3:H with excellent optoelectronic properties, prepared by atomic layer deposition at a temperature of 100 °C, has been made applicable to silicon heterojunction solar cells with a-Si:H p-layer. A mild O_2 or Ar plasma pretreatment of the a-Si:H surface promotes the adsorption of InCp molecules on the substrate. Under mild plasma conditions of high pressure and low power it is shown that vacuum ultraviolet radiation is responsible for the plasma-induced degradation of c-Si/a-Si:H interface passivation. This degradation can however be completely repaired by post-annealing. Finally, using a remote inductively coupled Ar plasma (120 s, 100 W, and 109 mTorr) for the surface pretreatment, an ALD In_2O_3:H window electrode has been implemented onto SHJ solar cells, demonstrating a high photocurrent density of 40.1 mA/cm^2 as determined from external quantum efficiency. The high photocurrent stems from a substantially reduced parasitic absorption in the entire wavelength range of 400–1200 nm for the In_2O_3:H compared to the case with ITO prepared by sputtering.

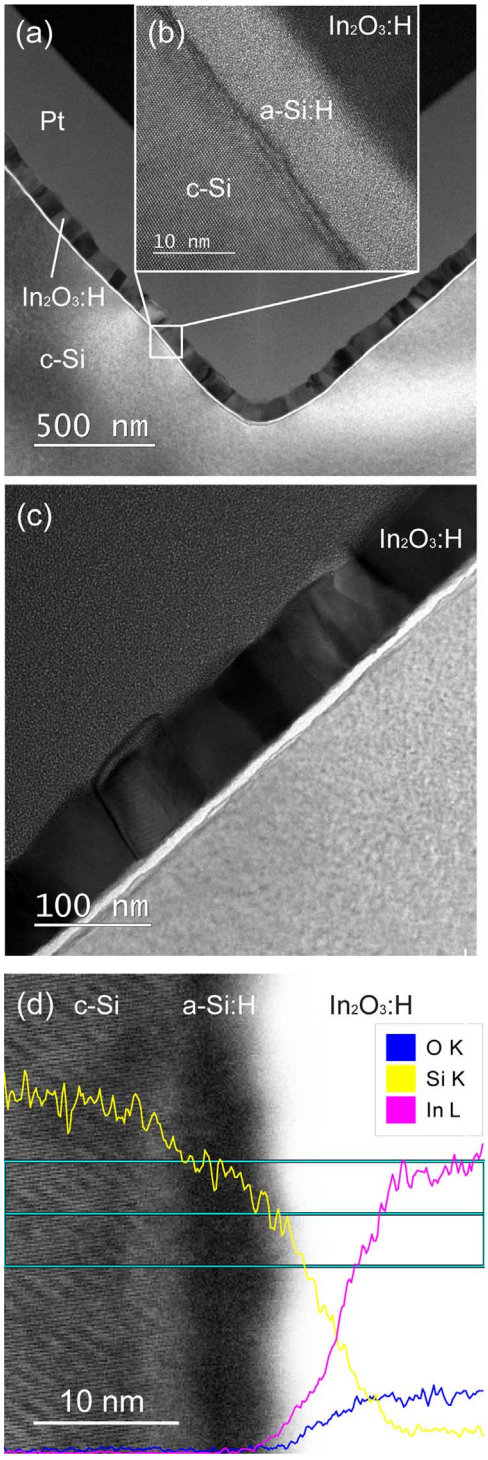

Fig. 8. (a) Bright field cross-sectional TEM image of a crystallized In_2O_3:H in the SHJ solar cell shown in Fig. 7. (b) The corresponding high-resolution TEM image. (c) Zoomed-in TEM image showing the grains of In_2O_3:H. (d) Compositional profiles at the c-Si/a-Si:H/In_2O_3:H interfaces, constructed from a 2-dimensional EDX map by averaging over the area indicated by the dark cyan box. (For interpretation of the references to color in this figure legend, the reader is referred to the web version of this article.)

Acknowledgements

We gratefully acknowledge Dr. H. Profijt for optical emission spectroscopy measurements, Dr. B. Barcones for the FIB preparation of the TEM sample, C.A.A. van Helvoirt and J. van Gerwen for technical assistance. This research is part of the FLASH program, which is financially supported by the Dutch Technology Foundation STW. The

Dutch province of Noord-Brabant and Solliance, a solar energy R & D initiative of ECN, Forschungszentrum Jülich, Holst Centre, IMEC, TNO, and TU/e, are acknowledged for funding the TEM facility.

Appendix A. Supporting information

Supplementary data associated with this article can be found in the online version at doi:10.1016/j.solmat.2017.01.011.

References

[1] M. Taguchi, A. Yano, S. Tohoda, K. Matsuyama, Y. Nakamura, T. Nishiwaki, K. Fujita, E. Maruyama, 24.7% Record efficiency HIT solar cell on thin silicon wafer, IEEE J. Photovolt. 4 (2014) 96–99. http://dx.doi.org/10.1109/JPHOTOV.2013.2282737.

[2] Z.C. Holman, A. Descoeudres, L. Barraud, F.Z. Fernandez, J.P. Seif, S. De Wolf, C. Ballif, Current losses at the front of Silion heterojunction solar cells, IEEE J. Photovolt. 2 (2012) 7–15. http://dx.doi.org/10.1109/JPHOTOV.2011.2174967.

[3] K. Ellmer, R. Mientus, Carrier transport in polycrystalline transparent conductive oxides: a comparative study of zinc oxide and indium oxide, Thin Solid Films 516 (2008) 4620–4627. http://dx.doi.org/10.1016/j.tsf.2007.05.084.

[4] L. Barraud, Z.C. Holman, N. Badel, P. Reiss, A. Descoeudres, C. Battaglia, S. De Wolf, C. Ballif, Hydrogen-doped indium oxide/indium tin oxide bilayers for high-efficiency silicon heterojunction solar cells, Sol. Energy Mater. Sol. Cells 115 (2013) 151–156. http://dx.doi.org/10.1016/j.solmat.2013.03.024.

[5] C. Battaglia, L. Erni, M. Boccard, L. Barraud, J. Escarré, K. Söderström, G. Bugnon, A. Billet, L. Ding, M. Despeisse, F.J. Haug, S. De Wolf, C. Ballif, Micromorph thin-film silicon solar cells with transparent high-mobility hydrogenated indium oxide front electrodes, J. Appl. Phys. 109 (2011) 114501. http://dx.doi.org/10.1063/1.3592885.

[6] T. Koida, H. Fujiwara, M. Kondo, Hydrogen-doped In_2O_3 as high-mobility transparent conductive oxide, Jpn. J. Appl. Phys. 46 (2007) L685–L687. http://dx.doi.org/10.1143/JJAP.46.L685.

[7] T. Koida, H. Fujiwara, M. Kondo, High-mobility hydrogen-doped In_2O_3 transparent conductive oxide for a-Si:H/c-Si heterojunction solar cells, Sol. Energy Mater. Sol. Cells 93 (2009) 851–854. http://dx.doi.org/10.1016/j.solmat.2008.09.047.

[8] B. Macco, Y. Wu, D. Vanhemel, W.M.M. Kessels, High mobility In_2O_3:H transparent conductive oxides prepared by atomic layer deposition and solid phase crystallization, Phys. Status Solidi - Rapid Res. Lett. 8 (2014) 987–990. http://dx.doi.org/10.1002/pssr.201409426.

[9] T. Koida, H. Fujiwara, M. Kondo, Reduction of optical loss in hydrogenated amorphous silicon/crystalline silicon heterojunction solar cells by high-mobility hydrogen-doped In_2O_3 transparent conductive oxide, Appl. Phys. Express 1 (2008) 041501. http://dx.doi.org/10.1143/APEX.1.041501.

[10] J. Geissbühler, J. Werner, S. Martin de Nicolas, L. Barraud, A. Hessler-Wyser, M. Despeisse, S. Nicolay, A. Tomasi, B. Niesen, S. De Wolf, C. Ballif, 22.5% Efficient silicon heterojunction solar cell with molybdenum oxide hole collector, Appl. Phys. Lett. 107 (2015) 081601. http://dx.doi.org/10.1063/1.4928747.

[11] T. Koida, H. Sai, M. Kondo, Application of hydrogen-doped In_2O_3 transparent conductive oxide to thin-film microcrystalline Si solar cells, Thin Solid Films 518 (2010) 2930–2933. http://dx.doi.org/10.1016/j.tsf.2009.08.060.

[12] T. Jäger, Y.E. Romanyuk, S. Nishiwaki, B. Bissig, F. Pianezzi, P. Fuchs, C. Gretener, M. Döbeli, A.N. Tiwari, Hydrogenated indium oxide window layers for high-efficiency Cu(In,Ga)Se_2 solar cells, J. Appl. Phys. 117 (2015) 205301. http://dx.doi.org/10.1063/1.4921445.

[13] J. Keller, J. Lindahl, M. Edoff, L. Stolt, T. Törndahl, Potential gain in photocurrent generation for Cu(In,Ga) Se_2 solar cells by using In_2O_3 as a transparent conductive oxide layer, Prog. Photovolt. Res. Appl. 24 (2015) 102–107. http://dx.doi.org/10.1002/pip.2655.

[14] F. Fu, T. Feurer, T. Jäger, E. Avancini, B. Bissig, S. Yoon, S. Buecheler, A.N. Tiwari, Low-temperature-processed efficient semi-transparent planar perovskite solar cells for bifacial and tandem applications, Nat. Commun. 6 (2015) 1–9. http://dx.doi.org/10.1038/ncomms9932.

[15] G. Yin, A. Steigert, P. Manley, R. Klenk, M. Schmid, Enhanced absorption in tandem solar cells by applying hydrogenated In_2O_3 as electrode, Appl. Phys. Lett. 107 (2015) 211901. http://dx.doi.org/10.1063/1.4936328.

[16] J. Werner, C.H. Weng, A. Walter, L. Fesquet, J.P. Seif, S. De Wolf, B. Niesen, C. Ballif, Efficient monolithic perovskite/silicon tandem solar cell with cell area > 1 cm^2, J. Phys. Chem. Lett. 7 (2016) 161–166. http://dx.doi.org/10.1021/acs.jpclett.5b02686.

[17] B. Demaurex, S. De Wolf, A. Descoeudres, Z.C. Holman, C. Ballif, Damage at hydrogenated amorphous/crystalline silicon interfaces by indium tin oxide overlayer sputtering, Appl. Phys. Lett. 101 (2012) 171604. http://dx.doi.org/10.1063/1.4764529.

[18] B. Macco, D. Deligiannis, S. Smit, R.A.C.M.M. van Swaaij, M. Zeman, W.M.M. Kessels, Influence of transparent conductive oxides on passivation of a-Si:H/c-Si heterojunctions as studied by atomic layer deposited Al-doped ZnO, Semicond. Sci. Technol. 29 (2014) 122001. http://dx.doi.org/10.1088/0268-1242/29/12/122001.

[19] B. Demaurex, J.P. Seif, S. Smit, B. Macco, W.M.M. Kessels, J. Geissbühler, S. De Wolf, C. Ballif, Atomic-layer-deposited transparent electrodes for silicon heterojunction solar cells, IEEE J. Photovolt. 4 (2014) 1387–1396. http://dx.doi.org/10.1109/JPHOTOV.2014.2344771.

[20] J.A. Libera, J.N. Hryn, J.W. Elam, Indium oxide atomic layer deposition facilitated by the synergy between oxygen and water, Chem. Mater. 23 (2011) 2150–2158. http://dx.doi.org/10.1021/cm103637t.

[21] B. Macco, H.C.M. Knoops, W.M.M. Kessels, Electron scattering and doping mechanisms in solid phase crystallized In2O3:H prepared by atomic layer deposition, ACS Appl. Mater. Interfaces 7 (2015) 16723–16729. http://dx.doi.org/10.1021/acsami.5b04420.

[22] P. Hohenberg, W. Kohn, Inhomogeneous electron gas, Phys. Rev. 136 (1964) 864–871. http://dx.doi.org/10.1103/PhysRev.136.B864.

[23] W. Kohn, L.J. Sham, Self-consistent equations including exchange and correlation effects, Phys. Rev. 140 (1965) 1133–1138. http://dx.doi.org/10.1103/PhysRev.140.A1133.

[24] J.P. Perdew, K. Burke, M. Ernzerhof, Generalized gradient approximation made simple, Phys. Rev. Lett. 77 (1996) 3865–3868. http://dx.doi.org/10.1103/PhysRevLett.77.3865.

[25] J.P. Perdew, K. Burke, M. Ernzerhof, Generalized gradient approximation made simple [Phys. Rev. Lett. 77, 3865 (1996)], Phys. Rev. Lett. 78 (1997). http://dx.doi.org/10.1103/PhysRevLett.78.1396.

[26] S. Grimme, J. Antony, S. Ehrlich, H. Krieg, A consistent and accurate ab initio parametrization of density functional dispersion correction (DFT-D) for the 94 elements H-Pu, J. Chem. Phys. 132 (2010) 154104. http://dx.doi.org/10.1063/1.3382344.

[27] T.P.M. Goumans, A. Wander, W.A. Brown, C.R.A. Catlow, Structure and stability of the (001) α-quartz surface, Phys. Chem. Chem. Phys. 9 (2007) 2146–2152. http://dx.doi.org/10.1039/B701176H.

[28] A. Thøgersen, S. Diplas, J. Mayandi, T. Finstad, A. Olsen, J.F. Watts, M. Mitome, Y. Bando, An experimental study of charge distribution in crystalline and amorphous Si nanoclusters in thin silica films, J. Appl. Phys. 103 (2008) 024308. http://dx.doi.org/10.1063/1.2832630.

[29] F.J. Himpsel, F.R. McFeely, A. Taleb-Ibrahimi, J.A. Yarmoff, G. Hollinger, Microscopic structure of the SiO_2/Si interface, Phys. Rev. B. 38 (1988) 6084–6096. http://dx.doi.org/10.1103/PhysRevB.38.6084.

[30] G. Hollinger, F.J. Himpsel, Probing the transition layer at the SiO_2-Si interface using core level photoemission, Appl. Phys. Lett. 44 (1984) 93–95. http://dx.doi.org/10.1063/1.94565.

[31] F. Lebreton, S.N. Abolmasov, F. Silva, P. Roca i Cabarrocas, In situ photoluminescence study of plasma-induced damage at the a-Si:H/c-Si interface, Appl. Phys. Lett. 108 (2016) 051603. http://dx.doi.org/10.1063/1.4941298.

[32] H. Plagwitz, B. Terheiden, R. Brendel, Staebler-Wronski-like formation of defects at the amorphous-silicon-crystalline silicon interface during illumination, J. Appl. Phys. 103 (2008) 094506. http://dx.doi.org/10.1063/1.2913320.

[33] S. De Wolf, B. Demaurex, A. Descoeudres, C. Ballif, Very fast light-induced degradation of a-Si:H/c-Si(100) interfaces, Phys. Rev. B. 83 (2011) 233301. http://dx.doi.org/10.1103/PhysRevB.83.233301.

[34] A. Illiberi, P. Kudlacek, A.H.M. Smets, M. Creatore, M.C.M. van de Sanden, Effect of ion bombardment on the a-Si:H based surface passivation of c-Si surfaces, Appl. Phys. Lett. 98 (2011) 242115. http://dx.doi.org/10.1063/1.3601485.

[35] H.B. Profijt, P. Kudlacek, M.C.M. van de Sanden, W.M.M. Kessels, Ion and photon surface interaction during remote plasma ALD of metal oxides, J. Electrochem. Soc. 158 (2011) G88–G91. http://dx.doi.org/10.1149/1.3552663.

[36] S. De Wolf, M. Kondo, Abruptness of a-Si:H/c-Si interface revealed by carrier lifetime measurements, Appl. Phys. Lett. 90 (2007) 042111. http://dx.doi.org/10.1063/1.2432297.